Effect of GaInP and GaAsP inserted into waveguide/barrier interface on carrier leakage in InAlGaAs quantum well 808-nm laser diode

FU Meng-jie, DONG Hai-liang, JIA Zhi-gang, JIA Wei, LIANG Jian, XU Bing-she

Citation:
FU Meng-jie, DONG Hai-liang, JIA Zhi-gang, JIA Wei, LIANG Jian, XU Bing-she. Effect of GaInP and GaAsP inserted into waveguide/barrier interface on carrier leakage in InAlGaAs quantum well 808–nm laser diode[J]. *Chinese Optics*, 2025, 18(1): 1–12. doi: 10.37188/CO.EN–2024–0006
付梦洁, 董海亮, 贾志刚, 贾伟, 梁建, 许并社. 波导/势垒界面插入GaInP和GaAsP对InAlGaAs量子阱808–nm半导体激光器载流子泄漏的影响[J]. 中国光学, 2025, 18(1): 1–12. doi: 10.37188/CO.EN–2024–0006

View online: https://doi.org/10.37188/CO.EN–2024–0006

文章编号　2097-1842(2025)01-0001-12

Effect of GaInP and GaAsP inserted into waveguide/barrier interface on carrier leakage in InAlGaAs quantum well 808-nm laser diode

FU Meng-jie[1], DONG Hai-liang[1,2*], JIA Zhi-gang[1], JIA Wei[1,2], LIANG Jian[3], XU Bing-she[1,2,4*]

(1. *Key Laboratory of Interface Science and Engineering in Advanced Materials*, *Ministry of Education*, *Taiyuan University of Technology*, *Taiyuan* 030024, *Shanxi*;

2. *Shanxi-Zheda Institute of Advanced Materials and Chemical Engineering*, *Taiyuan* 030024, *P. R. Shanxi*;

3. *College of Materials Science and Engineering*, *Taiyuan University of Technology*, *Taiyuan* 030024, *Shanxi*;

4. *Institute of Atomic and Molecular Science*, *Shaanxi University of Science & Technology*, *Xian* 710021, *Shaanxi*)

* *Corresponding author*, *E-mail*: *dhltyut@*163.*com*; *xubs@tyut.edu.cn*

Abstract: There is nonradiative recombination in waveguide region owing to severe carrier leakage, which in turn reduces output power and wall-plug efficiency. In this paper, we designed a novel epitaxial structure, which suppresses carrier leakage by inserting n-$Ga_{0.55}In_{0.45}P$ and p-$GaAs_{0.6}P_{0.4}$ between barriers and waveguide layers, respectively, to modulate the energy band structure and to increase the height of barriers. The results show that the leakage current density reduces by 87.71%, compared to traditional structure. The nonradiative recombination current density of novel structure reduces to 37.411 A/cm^2, and the output power reaches 12.80 W with wall-plug efficiency of 78.24% at an injection current density 5 A/cm^2 at room temperature. In addition, the temperature drift coefficient of center wavelength is 0.206 nm/°C at the temperature range from 5 °C to 65 °C, and the slope of fitted straight line of threshold current with temperature variation is 0.00113. The novel epitaxial structure provides a theoretical basis for achieving high-power laser diode.

Key words: 808-nm laser diode; $Ga_{0.55}In_{0.45}P$ and $GaAs_{0.6}P_{0.4}$ insertion layers; InAlGaAs quantum well; carrier leakage

收稿日期：2024-02-27；**修订日期**：xxxx-xx-xx

基金项目：国家自然科学基金（No. 61904120, No. 21972103）；山西省“1331 项目”和山西浙大新材料与化工研究院项目（No. 2022SX-TD018, No. 2021SX-AT001, 002 和 003）

Supported by National Natural Science Foundation of China (No. 61904120, No. 21972103); Shanxi “1331 project” and the Shanxi-Zheda Institute of Advanced Materials and Chemical Engineering (No. 2022SX-TD018, No. 2021SX-AT001, 002 and 003)

波导/势垒界面插入 GaInP 和 GaAsP 对 InAlGaAs 量子阱 808-nm 半导体激光器载流子泄漏的影响

付梦洁[1], 董海亮[1,2*], 贾志刚[1], 贾　伟[1,2], 梁　建[3], 许并社[1,2,4*]
（1. 太原理工大学 新材料界面科学与工程教育部重点实验室, 山西太原 030024;
2. 山西浙大新材料与化工研究院, 山西太原 030024;
3. 太原理工大学 材料科学与工程学院, 山西太原 030024;
4. 陕西科技大学 原子与分子科学研究所, 陕西西安 710021）

摘要: 传统半导体激光器由于载流子泄漏严重, 在波导区域发生非辐射复合, 进而降低了输出功率和电光转换效率。本文设计了一种新型外延结构, 通过在有源区两侧势垒和波导层之间分别插入 n-$Ga_{0.55}In_{0.45}P$ 和 p-$GaAs_{0.6}P_{0.4}$ 材料, 调控能带结构, 增大了阻挡载流子泄漏的势垒高度, 抑制了载流子泄漏。研究结果表明, 相较于传统结构器件, 泄漏电流密度降低了 87.71%。在 25 °C 注入电流密度为 5 A/cm² 时, 新型外延结构的非辐射复合电流密度降低至 37.411 A/cm², 输出功率达 12.80 W, 电光转换效率达 78.24%。此外, 在 5 °C~65 °C 温度变化范围内, 中心波长的温漂系数为 0.206 nm/°C, 阈值电流随温度变化的拟合直线的斜率为 0.001 13。本文所设计结构为抑制载流子泄漏提供了理论依据。

关　键　词: 808-nm 半导体激光器; $Ga_{0.55}In_{0.45}P$ 和 $GaAs_{0.6}P_{0.4}$ 插入层; InAlGaAs 量子阱; 载流子泄漏
中图分类号: TN248.4　**文献标志码:** A　**doi:** 10.37188/CO.EN-2024-0006　**CSTR:** 32171.14.CO.EN-2024-0006

1 Introduction

Laser diodes (LDs) are used in extreme conditions such as very high or low temperatures owing to their low voltage operating characteristics, high efficiency and reliability, and long lifetime[1]. LDs have excellent performance and are widely used in various fields, including medical aesthetics, laser welding, laser guidance, laser ignition, and most importantly as a pumping source for solid-state lasers[2]. However, as the demand for 808 nm LD applications expands, the performance requirements for LD are becoming increasingly stringent, particularly in terms of high output power, high wall-plug efficiency (WPE), superior beam quality, and reliability[3-5].

In traditional high-power LD, there is a problem known as carrier leakage, which can increase nonradiative recombination in waveguide region, leading to decreased output power, WPE, and stability[6]. Over the past few years, researchers have conducted numerous studies to reduce carrier leakage. Zhang B et al. inserted GaAs intermediate layer into InGaAs/AlGaAs multi-quantum wells, which reduced carrier leakage and ensured more radiative recombination in multi-quantum wells[7]; Cao Y L et al. inserted thin GaAsP interlayer into InGaAsP/InGaP/AlGaAs LD to optimize epitaxial structure and obtain strong carrier confinement[8]; Li X et al. added low Al content AlGaAs interlayer between active region and n-side waveguide, and the electron leakage was remarkably depressed, owing to the reduction of injected electron energy and the improvement of quantum well capture efficiency[9]; Asryan L V *et al.* adopted $Ga_{0.55}In_{0.45}P$ and $In_{0.22}Al_{0.42}Ga_{0.36}As$ as asymmetric barrier layers with electron and hole barrier heights of 78 and 240 meV, and compared to original structure, designed structure prevented hole leakage into waveguide layer resulting in low threshold current[10]; Zubov F I et al. adopted $Ga_{0.83}In_{0.17}P_{0.79}Sb_{0.21}$ and $Ga_{0.47}In_{0.53}P$ as barrier layers, which suppressed the fluxes of electrons and holes and significantly improved WPE[11]; Zhang X et al. used GaInAsP/GaAsP as asymmetric barrier with electron and hole leakage barrier heights

2.22 and 1.76 times higher than conventional structure[12]; Yuan Q H et al. inhibited carrier leakage in active region by adding GaAsP materials between barrier and waveguide layers for improving the temperature characteristics of LD[13]. From previous studies, we find that researchers have significantly increased the carrier leakage barrier height by adding insertion layer or adopting asymmetric barrier, which enhances the confinement of carriers in active region, reduces carrier leakage. Therefore, adding insertion layer or adopting asymmetric barrier is an effective way to reduce carrier leakage and improve optoelectronic performance. In this paper, we optimize the epitaxial structure by adding $Ga_{0.55}In_{0.45}P$ and $GaAs_{0.6}P_{0.4}$ insertion layers. This approach reduces carrier leakage, decreases the device's series resistance, and enhances its temperature characteristics. However, the mechanism of adding insertion layer and its effect on carrier leakage need to be further studied.

A novel 808 nm LD is proposed in order to reduce carrier leakage by inserting $Ga_{0.55}In_{0.45}P$ and $GaAs_{0.6}P_{0.4}$ layers between barrier and waveguide layers on both sides of active region. $Ga_{0.55}In_{0.45}P$ and $GaAs_{0.6}P_{0.4}$ materials possess wide bandgaps, providing strong confinement for electrons and holes. This effectively blocks carrier leakage, reduces nonradiative recombination in waveguide region, and utilizes high carrier confinement to achieve favorable temperature characteristics. Moreover, the novel LD not only can enhance optical field limiting capacity but also reduce optical loss by increasing refractive index gap between waveguide and active regions. The relationship between optoelectronic performance and structure is discussed by comparing with and without insertion layers.

2 Design of epitaxial structure

InAlGaAs/AlGaAs active region was used for 808 nm LD. AlGaAs, a commonly used material, was used for barrier, waveguide, and cladding layers of LD1 structure, as shown in Figure 1. First, we optimized content and thickness of each layer of traditional LD1, and obtained its optimal structural parameters as 2000 nm-thick n-GaAs substrate and 350 nm-thick p-GaAs contact layer, 1 200 nm-thick n-type $Al_{0.55}Ga_{0.45}As$ cladding layer and 1 000 nm-thick p-type $Al_{0.55}Ga_{0.45}As$ cladding layer, 600 nm-thick n-type and 300 nm-thick p-type $Al_{0.35\text{-}0.55}Ga_{0.65\text{-}0.45}As$ gradient waveguide layers, 6 nm-thick $Al_{0.2}Ga_{0.8}As$ barrier layers and 5 nm-thick $In_{0.14}Al_{0.16}Ga_{0.7}As$ quantum well (InAlGaAs has a high band step and thus will act as a good electron confinement and have a high temperature stability[14, 15]). In contrast to LD1, LD2 used 8 nm-thick $Ga_{0.55}In_{0.45}P$ as insertion layers between barrier and waveguide layers on both sides of active region. Designed structure LD3 used $Ga_{0.55}In_{0.45}P$ and $GaAs_{0.6}P_{0.4}$ as insertion layers between barrier and waveguide layers on both sides of active region, and only insertion layers material was optimized, while other parameters remain unchanged. The bandgap of $Ga_{0.55}In_{0.45}P$ and $GaAs_{0.6}P_{0.4}$ is larger than the bandgap of potential barrier, so that carriers in active region need higher energy to cross $Ga_{0.55}In_{0.45}P$ and $GaAs_{0.6}P_{0.4}$ insertion layers, thereby effectively suppresses carriers crossing barrier into cladding layer and generating nonradiative recombination. So we choose $Ga_{0.55}In_{0.45}P$ and $GaAs_{0.6}P_{0.4}$ insertion layers to optimize the epitaxial structure. Figure 1 (color online) displayed the particular parameters of three LDs epitaxial structures.

In this study, LD was simulated by the simulation software SiLENSe with six-by-six k·p method. In the simulation, the device cavity length and strip width were set to be 2000 μm and 100 μm, and the reflectivity of the front and back cavity surfaces were 10% and 98%, respectively. The nonradiative lifetimes of electron and hole were 5.0×10^{-9} s and 5.0×10^{-8} s, respectively, and the dislocation density was 100 cm^{-2}. The specific parameter values used for the devices in the simulation were shown in Table 1.

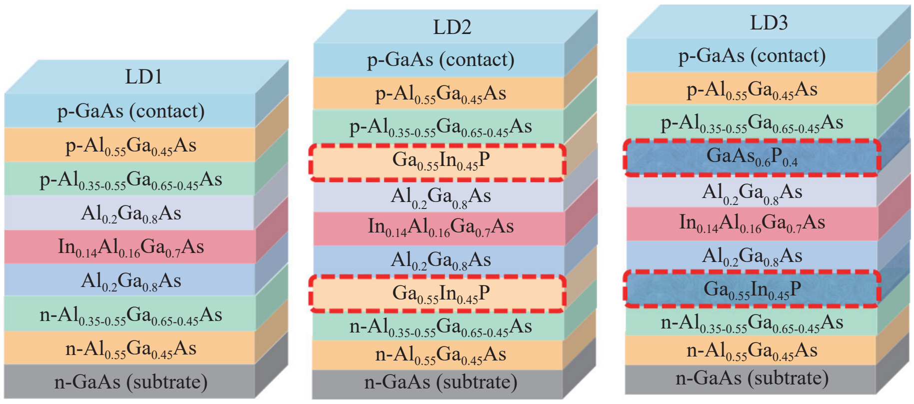

Fig. 1 Diagram of three LDs' epitaxial structures

Tab. 1 Parameters of 808-nm LD's epitaxial structures

Structure	Materials	Thicknesses /nm	Doping concentration /cm^{-3}
p-Contact layer	GaAs	350	1×10^{19}
p-Cladding layer	$Al_{0.55}Ga_{0.45}As$	1 000	1×10^{19}
p-Waveguide layer	$Al_{0.35\text{-}0.55}Ga_{0.65\text{-}0.45}As$	300	1×10^{17}~1×10^{18}
p-Insertion layer	$Ga_{0.55}In_{0.45}P/GaAs_{0.6}P_{0.4}$	8	1×10^{17}
p-Barrier layer	$Al_{0.2}Ga_{0.8}As$	6	0
Quantum well	$In_{0.14}Al_{0.16}Ga_{0.7}As$	5	0
n-Barrier layer	$Al_{0.2}Ga_{0.8}As$	6	0
n-Insertion layer	$Ga_{0.55}In_{0.45}P$	8	1×10^{17}
n-Waveguide layer	$Al_{0.35\text{-}0.55}Ga_{0.65\text{-}0.45}As$	600	1×10^{17}~1×10^{18}
n-Cladding layer	$Al_{0.55}Ga_{0.45}As$	1 200	1×10^{19}
n-Substrate	GaAs	2000	1×10^{19}

3 Simulation results and analysis

3.1 Optical Properties

We investigated the effect of inserting $Ga_{0.55}In_{0.45}P$ and $GaAs_{0.6}P_{0.4}$ materials on refractive index and optical field distribution of three LDs, as shown in Figure 2(a) (color online). Figure 2(b) (color online) is an enlarged figure in the range of 1 750−1 900 nm. Optical loss for carrier absorption on n-side is lower than on p-side region during photon transmission, and adjusting optical field distribution to shift toward n-side in order to reduce optical loss[16]. Traditional and designed LDs have adopted an asymmetric structure for both waveguide thickness and cladding layer thickness, which is effective in reducing p-side optical loss[16, 17]. With insertions of $Ga_{0.55}In_{0.45}P$ and $GaAs_{0.6}P_{0.4}$ between barrier and waveguide layers on both sides, it is found that refractive index differential between active region and waveguide layer become larger so that limiting optical field enhanced and photon leakage reduced, resulting in low optical loss. As shown in Figure 2(b), the refractive index differential between barrier and waveguide layer of LD1 is 0.101, while for LD3 the refractive index differential between p-side insertion layer and the waveguide layer increases to 0.121. The asymmetric refractive index distribution keeps optical modes away from p-side, and increasing refractive index on p-side results in enhanced optical field limitation, all of which lead to a decrease in free carrier induced optical absorption in high doped p-cladding layer. Therefore, designed structure LD3 increases refractive index differential between active region and waveguide layer, which reduces optical absorption in cladding layer and decreases optical loss.

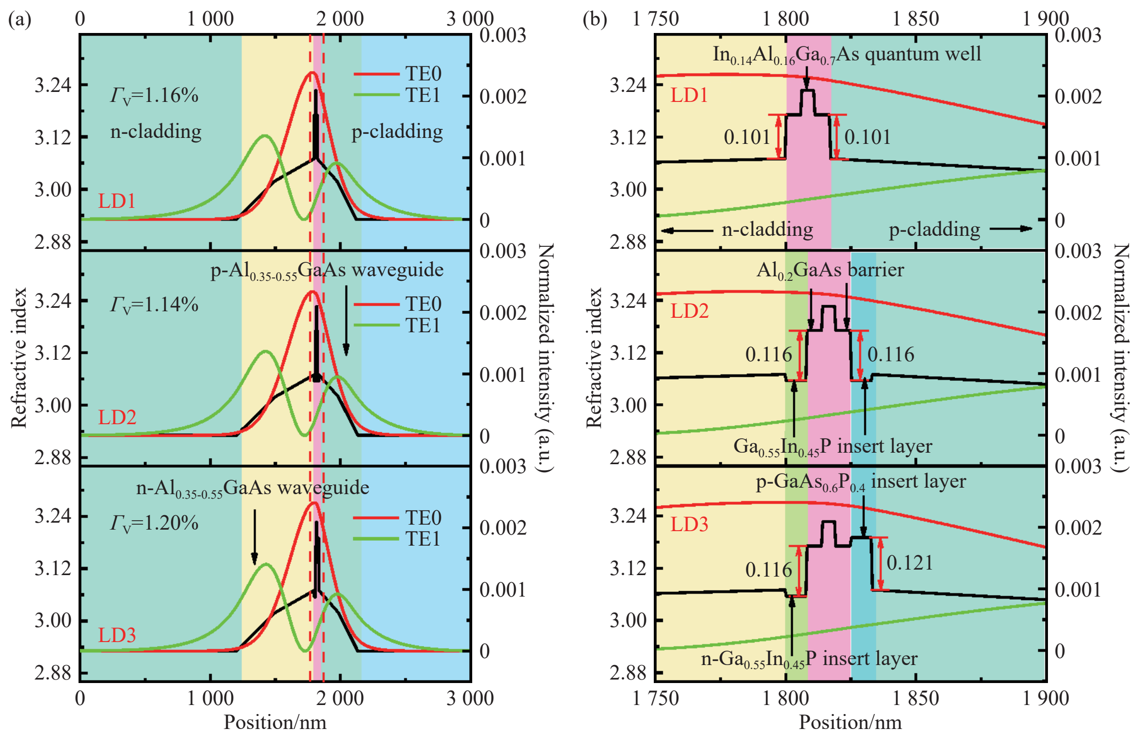

Fig. 2　(a) Refractive index and TE mode optic field intensity distributions of three LDs; (b) magnified diagrams in the range of 1 750−1 900 nm for LD1, LD2, and LD3

Reducing optical loss in epitaxial structure is a key factor for achieving high output power[18-19]. In order to investigate the effect of $Ga_{0.55}In_{0.45}P$ and $GaAs_{0.6}P_{0.4}$ insertion layers on optical loss, we explore the variation of optical loss caused by free carrier absorption of three LDs, as shown in Figure 3 (color online). Figure 3(a) demonstrates optical loss owing to free carrier absorption outside of quantum well for three LDs. Optical loss outside (α_{Out}) of quantum well are 0.281, 0.262 and 0.254 cm^{-1} for LD1, LD2 and LD3. The difference in α_{Out} between LD1 and LD3 is 0.027 cm^{-1}. Insertion of $GaAs_{0.6}P_{0.4}$ intermediate layer on p-side increases refractive index value between waveguide layer and active region, and the overlap between p-side optical field distribution and waveguide region decreases, thus reducing α_{Out}. Optical loss in quantum well (α_{QW}) of LD1, LD2 and LD3 are 0.060, 0.034 and 0.033 cm^{-1}, respectively, and the difference in α_{QW} between LD1 and LD3 is 0.027 cm^{-1}. Therefore, $Ga_{0.55}In_{0.45}P$ and $GaAs_{0.6}P_{0.4}$ insertion layers reduce its free carrier absorption and provide sufficient energy barriers to limit carrier leakage in active region. As shown in Figure 3(c), total optical loss (α_{Total}) of LD1, LD2 and LD3 are 6.648, 6.603, and 6.595 cm^{-1}, respectively. The difference between α_{Total} of LD1 and LD3 is 0.053 cm^{-1}. This value is approximately equal to the summation of the differential values of α_{Out} and α_{QW} of LD1 and LD3. Calculations reveal that the percentage variation of α_{Out} and α_{QW} accounts for 49.06% and 50.94% of the total variation in α_{Total}. Compared with LD1, quantum wells of LD2 and LD3 are shifted toward p-side by 8 nm, which solves the problem that absorption on the p-side is larger than n-side owing to the difference in the properties of electron and hole[20]. It reduces loss of p-side photons and decreases optical absorption loss of free carrier in waveguide region, which leads to a small reduction in α_{Total} and thus improves conversion efficiency[21]. Therefore p-side region is more critical for α_{QW}.

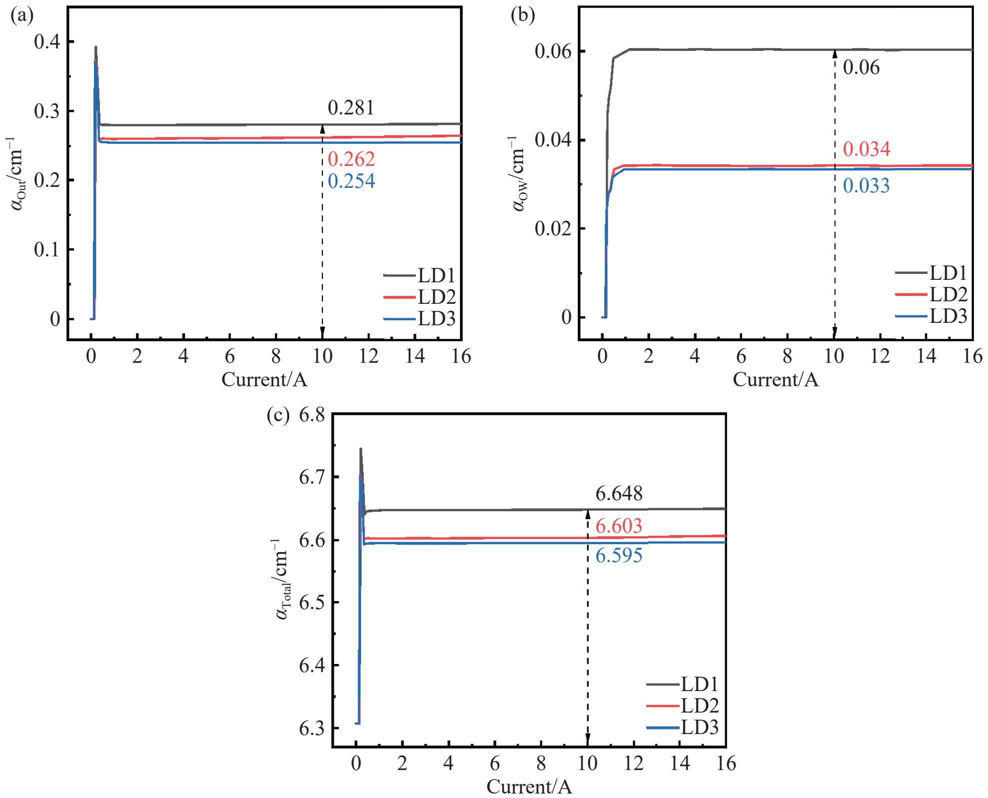

Fig. 3 Curves of (a) quantum well external loss (α_{Out}), (b) quantum well internal loss (α_{QW}), and (c) total optical loss (α_{Total}) of three LDs as a function of injection current

3.2 Electrical Properties

To investigate the effect of $Ga_{0.55}In_{0.45}P$ and $GaAs_{0.6}P_{0.4}$ insertion layers on carrier leakage, energy bands for three LDs are analyzed at injection current 5 kA/cm^2 (10 A), as shown in Figure 4(a) (color online). Figure 4(b) (color online) provides a magnified diagram of LD1, LD2 and LD3 in the range of 1 760−1 860 nm. By comparing LD1 and LD2 with LD3, it is found that the effective electron leakage height of LD1 is 338 meV and the effective hole leakage height is 405 meV. The effective electron leakage height and the effective hole leakage height of LD2 are 287 and 416 meV. LD3 has an effective electron leakage height and effective hole leakage height of 397 and 425 meV, respectively. It can be observed that the effective electron leakage height and the effective hole leakage height differences are 59 and 20 meV for LD1 and LD3, respectively. LD3 has a larger effective electron leakage height than effective hole leakage height compared to LD1, which solves the problem that electron migration rate is higher than hole migration rate at the same concentration owing to electron's effective mass being smaller than hole's effective mass[22]. The effective electron leakage height and the effective hole leakage height of LD3 are 1.17 and 1.05 times higher than that of LD1, increasing the effective blocking height between waveguide layer and cladding layer in n-type region and p-type region, preventing the escape of electron (hole) to p-cladding layer (n-cladding layer) and enhancing the restriction capability of carriers. Therefore, LD3 effectively suppresses the leakage of electron and hole into cladding region by increasing the heights of effective leakage barrier of electron and hole, which reduces nonradiative recombination, improves carrier utilization efficiency, and increases radiative recombination.

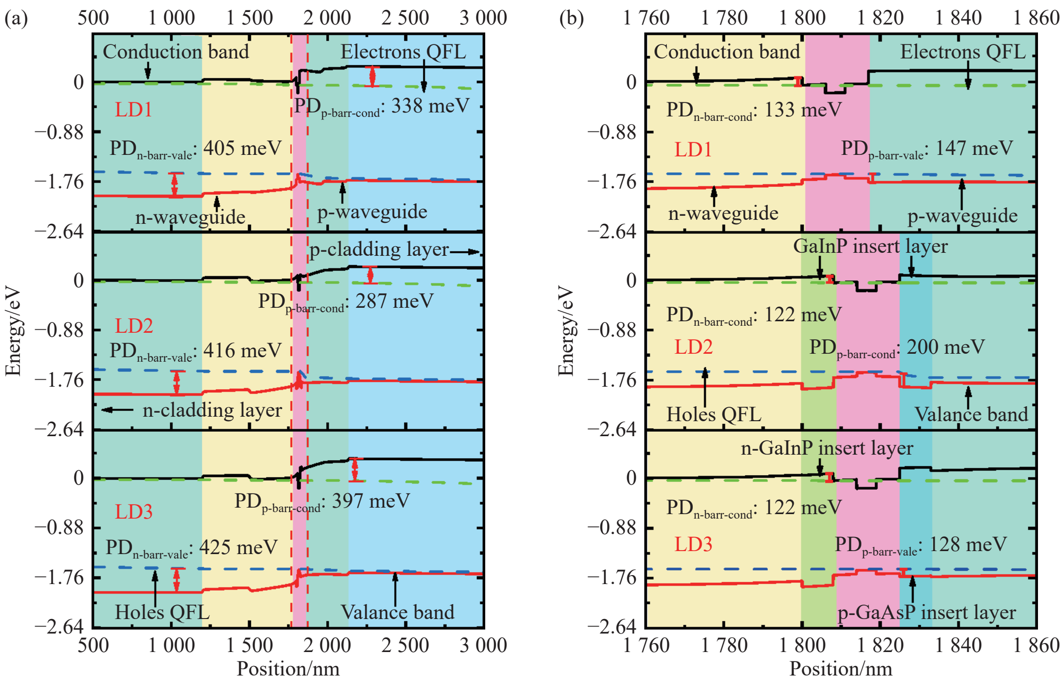

Fig. 4　(a) The energy band comparison of the LDs with three structures at an injection current of 10 A and (b) the magnification of LD1, LD2, and LD3 in the 1 760−1 860 nm range

We explore the effect of energy band on carrier transport in above part. It is found that increasing the effective leakage barrier heights of electron and hole is beneficial in enhancing confinement to carriers and reducing nonradiative recombination, which has an important effect on the improvement of the performance of LD[23]. Leakage current density, Auger recombination current density, SRH recombination current density, and nonradiative recombination current density versus injection current for three LDs are shown in Figure 5 (color online). From Figure 5(a), leakage current densities of LD1 and LD2 are 0.236 and 2.108 A/cm^2, leakage current density of LD3 is 0.029 A/cm^2, and LD3 reduces leakage current density by 87.71% compared to LD1, owing to enhanced carrier effective barrier height, leading to a reduction in carrier leakage. As shown in Figure 5(b), the Auger recombination current densities of LD1, LD2 and LD3 are 31.545, 37.796 and 30.931 A/cm^2 at injection current 10 A, the Auger recombination current densities of three LDs are almost constant in their values with increasing current. As shown in Figure 5(c), the SRH recombination current densities of three LDs are 20.172, 10.664 and 6.480 A/cm^2 at injection current 10 A, the SRH recombination current densities of LD1 and LD2 vary with injection current, and that of LD3 remains almost unchanged versus injection current. From Figure 5(d), it can be seen that the nonradiative recombination current densities of three LDs are 42.209, 57.969 and 37.411 A/cm^2 at injection current 10 A. Among them, the nonradiative recombination current densities of LD1 and LD2 increase with increasing injection current. While LD3 has a steady trend as current increases, and the nonradiative recombination current densities of LD1 is 1.11 times higher than that of LD3. Since LD3 optimizes carrier transport, nonradiative recombination current density and SRH recombination current density of LD3 remain almost constant as injection current increases[24].

In order to meet high efficiency and development of device, low threshold current and operating voltage, high output power and WPE are the main objectives of epitaxial structure design[25]. Figure 6 (color online) illustrates the relationship between threshold current, operating voltage, output power, and WPE versus injection current for three LDs. As depicted in Figure 6(a), threshold currents of three LDs are 0.511, 0.512 and 0.501 A, with LD3 showing a slightly low threshold current. When analyzing the optical performance, it is found that the optical limiting ability of LD3 is enhanced and the optical loss is reduced compared to LD1, so the reduction of threshold current is mainly from the decrease of carrier loss[24]. Figure 6(b) shows the variation curve of operating voltage with injection current, and the slope of I-V curve indicates the magnitude of series resistance. Operating voltages of three LDs are 1.702, 1.744 and 1.636 V, respectively, at injection current 10 A. It is clear that the operating voltage of LD3 is very low, mainly owing to the reduction of its series resistance. According to the series resistance formula, we know that the resistance is mainly determined by the thickness, doping concentration and carrier mobility. Owing to $Ga_{0.55}In_{0.45}P$ and $GaAs_{0.6}P_{0.4}$ are very thin, so their thickness is negligible, moreover $Ga_{0.55}In_{0.45}P$ and $GaAs_{0.6}P_{0.4}$ have large mobility and high doping concentration, resulting in low series resistance, which reduces the operating voltage of LD3. As illustrated in Figure 6(c), output power are 12.68, 12.66, and 12.80 W for three LDs at injection current 10 A, with LD3 having a high output power owing to low optical loss, threshold current, and operating voltage. Lastly, Figure 6(d) shows WPE of three LDs are 74.48%, 72.62%, and 78.24% at injection current 10 A. The WPE of LD3 is improved by 3.76% and 5.62% compared to LD1 and LD2, respectively. The addition of high doping and high mobility $Ga_{0.55}In_{0.45}P$ and $GaAs_{0.6}P_{0.4}$ insertion layers in LD3 leads to reduction in operating voltage and series resistance, which in turn improves the WPE. The WPE of LD1 is slightly higher than that of LD3 at current of 1-2 A owing to the abrupt change of refractive index at the interface of LD1, causing increased energy losses. However, as the injection current increases, the carrier loss generated in the device operation decreases, and the high power and high WPE are achieved by reducing optical and energy losses[26].

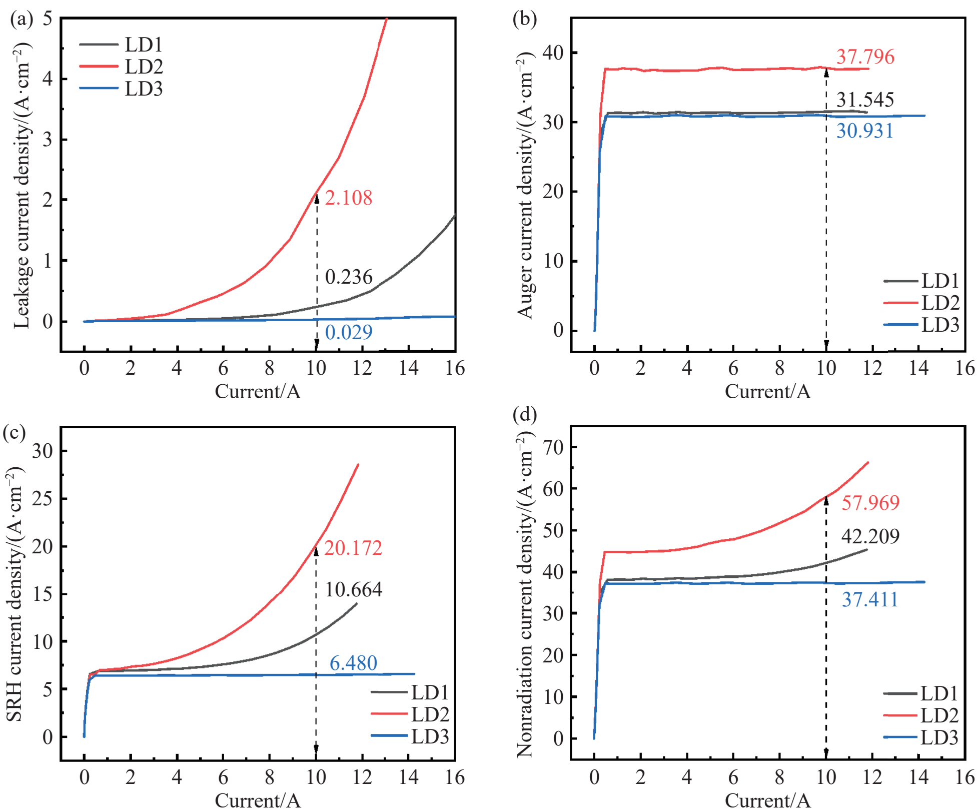

Fig. 5 (a) Leakage current density, (b) Auger recombination current density (c) SRH recombination current density, and (d) nonradiative recombination current density of three LDs as a function of injection current

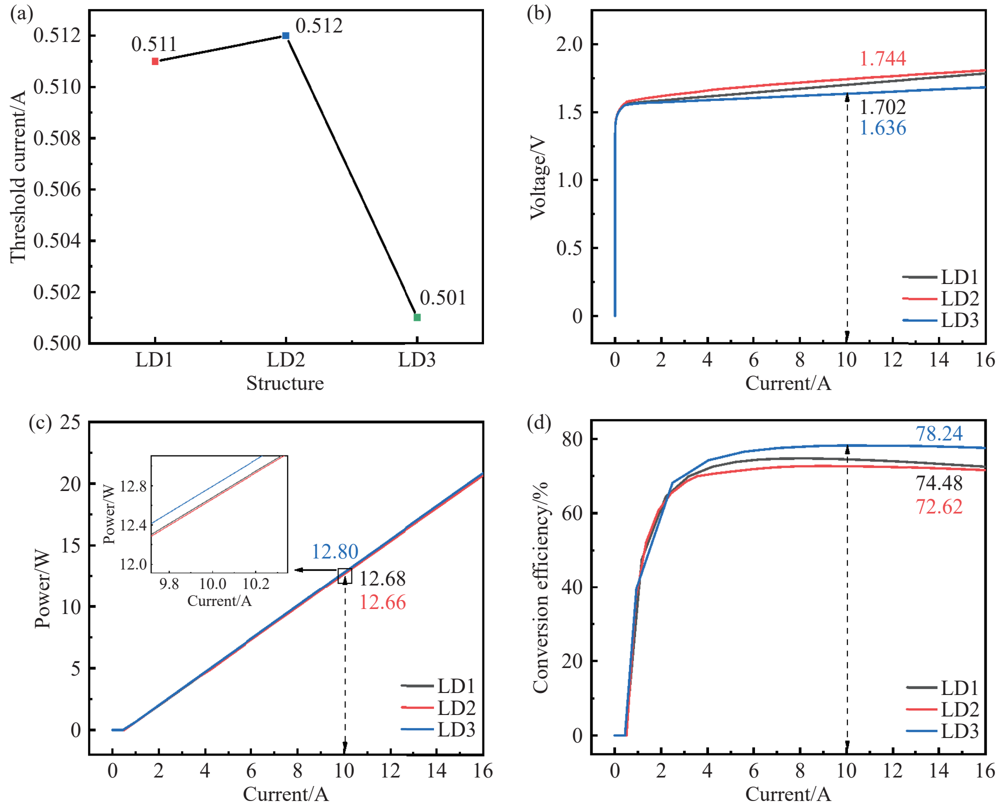

Fig. 6　(a) Threshold current of three LDs; (b) operating voltage, (c) output power and (d) WPE of three LDs as a function of injection current

3.3　Temperature Characteristics

The above discussion shows the optoelectronic performance of three LDs at room temperature of 25 °C. To evaluate the stability during operation, we simulated the variation rules of wavelength and threshold current of three LDs at different temperature. Graphs of wavelength and threshold current variation over the temperature ranged from 5 to 65 °C for three LDs are shown in Figure 7 (color online).

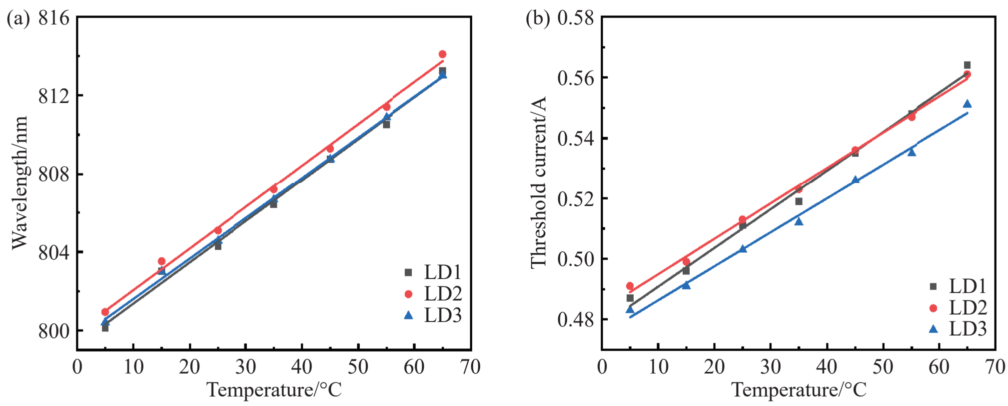

Fig. 7　(a) Fitted curves of wavelength and (b) threshold current of three LDs as a function of temperature

From Figure 7(a), it can be observed that three LDs exhibit red shift with increasing temperature owing to bandgap shrinking caused by Joule heating[27]. The temperature drift coefficients of LD1, LD2 and LD3 are 0.210, 0.212 and 0.206 nm/°C. LD1 and LD2 have poor wavelength stability at high temperature, whereas LD3 exhibits more stable wavelength owing to the addition of $Ga_{0.55}In_{0.45}P$ and $GaAs_{0.6}P_{0.4}$ insertion layers, which has a small temperature-drift coefficient at the center wavelength. Figure 7(b) reveals the graphs of threshold currents of three LDs over the range of temperature variations. Threshold currents gradually increase as increasing temperature. However, LD3 exhibits a low threshold current at the same temperature, and the slopes of the fitted straight lines of threshold current versus temperature are 0.001 28, 0.001 18, and 0.001 13 for three LDs. This indicates that LD3 has excellent threshold current stability during operation. From the above analysis, it can be seen that the center wavelength temperature drift coefficient of LD3 is smaller and the threshold current change is more stable than others. Therefore, LD3 has a slightly superior temperature dependence, which can reduces electron leakage, thereby improving the reliability[28]. So adding $Ga_{0.55}In_{0.45}P$ and $GaAs_{0.6}P_{0.4}$ insertion layers is instructive to improve the reliability.

4 Conclusion

In summary, based on InAlGaAs/AlGaAs active zone, $Ga_{0.55}In_{0.45}P$ and $GaAs_{0.6}P_{0.4}$ insertion layers between barrier layer and waveguide layer on both sides of active region changes energy band, which not only reduces carrier loss by resolving electron mobility larger than hole mobility but also decreases nonradiative recombination by increasing the height of effective carrier leakage barrier. Leakage current density decreases by 87.71%, and nonradiative recombination current density decreases to 37.411 A/cm^2. Output power and WPE reach 12.80 W and 78.24%, respectively, at injection current 10 A. In addition, temperature drift coefficient of the center wavelength is 0.206 nm/°C over the temperature variation range of 5 °C−65 °C.

References:

[1] CRUMP P, ERBERT G, WENZEL H, *et al*.. Efficient high-power laser diodes[J]. *IEEE Journal of Selected Topics in Quantum Electronics*, 2013, 19(4): 1501211.

[2] KAUSHAL H, KADDOUM G. Applications of lasers for tactical military operations[J]. *IEEE Access*, 2017, 5: 20736-20753.

[3] LI X Y, JIANG K, ZHU ZH, *et al*.. High-brightness 808 nm semiconductor laser diode packaged by SiC heat sink[J]. *Journal of Modern Optics*, 2020, 67(11): 1017-1021.

[4] REHIOUI O, BECHOU L, FILLARDET T, *et al*.. Degradation analysis of individual emitters in 808nm QCW laser diode array for space applications[J]. *Proceedings of SPIE*, 2010, 7583: 758314.

[5] WANG B G, TAN SH Y, ZHOU L, *et al*.. High reliability 808nm laser diodes with output power over 19W under CW operation[J]. *IEEE Photonics Technology Letters*, 2022, 34(6): 349-352.

[6] FREVERT C, CRUMP P, BUGGE F, *et al*.. The impact of low Al-content waveguides on power and efficiency of 9xx nm diode lasers between 200 and 300 K[J]. *Semiconductor Science and Technology*, 2016, 31(2): 025003.

[7] ZHANG B, WANG H ZH, WANG X, *et al*.. Effect of GaAs insertion layer on the properties improvement of InGaAs/AlGaAs multiple quantum wells grown by metal-organic chemical vapor deposition[J]. *Journal of Alloys and Compounds*, 2021, 872: 159470.

[8] CAO Y L, LIAN P, MA W Q, *et al*.. Influence of GaAsP insertion layers on performance of InGaAsP/InGaP/AlGaAs quantum-well laser[J]. *Chinese Physics Letters*, 2006, 23(9): 2583-2586.

[9] LI X, ZHAO D G, JIANG D SH, *et al*.. Suppression of electron leakage in 808 nm laser diodes with asymmetric waveguide layer[J]. *Journal of Semiconductors*, 2016, 37(1): 014007.

[10] ASRYAN L V, ZUBOV F I, KRYZHANOVSKAYA N V, *et al*.. Lasers with asymmetric barrier layers: a promising type of injection lasers[J]. *Journal of Physics: Conference Series*, 2016, 741: 012111.

[11] ZUBOV F I, MURETOVA M E, ASRYAN L V, *et al*.. Feasibility study for Al-free 808 nm lasers with asymmetric barriers suppressing waveguide recombination[J]. *Journal of Applied Physics*, 2018, 124(13): 133105.

[12] ZHANG X, DONG H L, JIA ZH G, *et al*.. Effect of $Ga_{1-x}In_xAs_{1-y}P_y$ Al-free asymmetric barrier on GaAs-based 808-nm laser diode[J]. *Optics Letters*, 2022, 47(5): 1153-1156.

[13] 袁庆贺, 井红旗, 仲莉, 等. 高功率高可靠性 9XX nm 激光二极管[J]. 中国激光, 2020, 47(4): 0401006.
YUAN Q H, JING H Q, ZHONG L, *et al*.. High-power and high-reliability 9XX-nm laser diode[J]. *Chinese Journal of Lasers*, 2020, 47(4): 0401006. (in Chinese).

[14] ZHANG J, NING Y Q, ZENG Y G, *et al*.. Design and analysis of high-temperature operating 795 nm VCSELs for chip-scale atomic clocks[J]. *Laser Physics Letters*, 2013, 10(4): 045802.

[15] ZHANG Y, NING Y Q, ZHANG L S, *et al*.. Design and comparison of GaAs, GaAsP and InGaAlAs quantum-well active regions for 808-nm VCSELs[J]. *Optics Express*, 2011, 19(13): 12569-12581.

[16] LAN Y, YANG G W, LIU Y X, *et al*.. 808 nm broad-area laser diodes designed for high efficiency at high-temperature operation[J]. *Semiconductor Science and Technology*, 2021, 36(10): 105012.

[17] SLIPCHENKO S O, VINOKUROV D A, PIKHTIN N A, *et al*.. Ultralow internal optical loss in separate-confinement quantum-well laser heterostructures[J]. *Semiconductors*, 2004, 38(12): 1430-1439.

[18] LIU Y X, YANG G W, ZHAO Y M, *et al*.. 48 W continuous-wave output from a high-efficiency single emitter laser diode at 915 nm[J]. *IEEE Photonics Technology Letters*, 2022, 34(22): 1218-1221.

[19] 曼玉选, 仲莉, 马骁宇, 等. 极低内部光学损耗 975 nm 半导体激光器[J]. 光学学报, 2020, 40(19): 1914001.
MAN Y X, ZHONG L, MA X Y, *et al*.. 975 nm semiconductor lasers with ultra-low internal optical loss[J]. *Acta Optica Sinica*, 2020, 40(19): 1914001. (in Chinese).

[20] AVRUTIN E A, RYVKIN B S, KOSTAMOVAARA J T. AlGaAs/GaAs asymmetric-waveguide, short cavity laser diode design with a bulk active layer near the *p*-cladding for high pulsed power emission[J]. *IET Optoelectronics*, 2021, 15(4): 194-199.

[21] RYVKIN B S, AVRUTIN E A. Asymmetric, nonbroadened large optical cavity waveguide structures for high-power long-wavelength semiconductor lasers[J]. *Journal of Applied Physics*, 2005, 97(12): 123103.

[22] ZUBOV F I, MURETOVA M E, PAYUSOV A S, *et al*.. Parasitic recombination in a laser with asymmetric barrier layers[J]. *Semiconductors*, 2020, 54(3): 366-373.

[23] ZHANG X L, DONG H L, ZHANG X, *et al*.. Reduction of nonradiative recombination for high-power 808 nm laser diode adopting InGaAsP/InGaAsP/GaAsP active region[J]. *Optics Communications*, 2023, 537: 129461.

[24] KHALFIN V B, GULAKOV A B, KOCHNEV I V, *et al*.. The influence of leakage on the characteristics of QW lasers[J]. *AIP Conference Proceedings*, 1991, 240(1): 49-57.

[25] KAIFUCHI Y, YOSHIDA K, YAMAGATA Y, *et al*.. Enhanced power conversion efficiency in 900-nm range single emitter broad stripe laser diodes maintaining high power operability[J]. *Proceedings of SPIE*, 2019, 10900: 109000F.

[26] XU B SH, QU K, WANG ZH Y, *et al*.. Investigation of photoelectric performance of laser diode by regulation of p-waveguide layer thickness[J]. *Optik*, 2020, 200: 163458.

[27] WU SH H, LI T, WANG ZH F, *et al*.. Study of temperature effects on the design of active region for 808 nm high-power semiconductor laser[J]. *Crystals*, 2023, 13(1): 85-99.

[28] WENZEL H, ERBERT G, BUGGE F, *et al*.. Optimization of GaAsP-QWs for high-power diode lasers at 800 nm[J]. *Proceedings of SPIE*, 2000, 3947: 32-38.

Author Biographies:

FU Meng-jie (1996—), female, born in Shangqiu, Henan Province. She received her bachelor's degree from Henan University of Urban Construction in 2020, and is now a master candidate in the School of Taiyuan University of Technology. She is mainly engaged in the design of epitaxial structure for 808 nm LD. E-mail: 2227240245@qq.com

DONG Hai-liang (1984—), born in Dongming country, Shandong province M. S. Supervisor. He received his B. S. degree from Ludong University in 2008, M. S. degree from Taiyuan University of Technology in 2011, and Ph. D. degree from Taiyuan University of Technology in 2016; Since 2019, he has been working as a senior experiment in the Key Laboratory of Interface Science and Engineering in Advanced Materials, Taiyuan University of Technology; His main research work is GaAs and GaN based semiconductor lasers, the Light-emitting device structure design, epitaxial material growth and performance characterization. E-mail: dhltyut@163.com

Mr. Xu Bingshe (1959 —), born in Yicheng City, Shanxi province, Professor and Doctoral Supervisor, received his Bachelor's Degree from Taiyuan University of Technology in 1978, and his Doctoral Degree from the University of Tokyo in 1994. He has presided and currently is working on more than 50 national and provincial projects, such as the National Outstanding Young Scientist Fund, the National 973 Program, the International Science and Technology Cooperation Program of the Ministry of Science and Technology, the Major Research Program of the National Natural Science Foundation of China (Nano Special Project), the National Natural Science Foundation of China, and the Sino-Japanese International Cooperation Program of the National Natural Science Foundation of China, and so on. His research interests include nano and thin film functional materials and their devices. He has published more than 450 papers in Advanced Functional Materials, Angewandte Chemie, Acta Materialia, and other national and international journals. E-mail: xubs@tyut.edu.cn